

The effect of oxide thickness on osteoblast attachment and survival on NiTi alloy

V. Muhonen · R. Heikkinen · A. Danilov ·
T. Jämsä · J. Tuukkanen

Received: 10 August 2005 / Accepted: 15 February 2006 / Published online: 13 January 2007
© Springer Science+Business Media, LLC 2007

Abstract NiTi alloy is used in various medical applications and the surface titanium oxide layer produced naturally or enhanced artificially has been thought to offer a protecting film against allergic and toxic effects of nickel (Ni). In this study, we investigated the effect of different oxide layer thicknesses on the survival and attachment of osteoblastic cells (ROS-17/2.8). AFM, X-ray diffraction and electrical resistance measurements were used to analyze the surface properties of oxidized NiTi samples and the effect of oxidation on material properties. The results clearly showed that straight correlation between oxide thickness and cellular well-being cannot be made. However, the different thicknesses of oxide layer on NiTi had surprising impacts on cellular responses and also to the properties of the metal alloy.

1 Introduction

Biomaterial technology aims to achieve new materials and tailor old ones in order to produce biomedical materials possessing properties that enable differentiation and assembly of cells to form tissues or to become biocompatible to the surrounding tissue [1].

Since cell adhesion, proliferation, differentiation, and metabolism as well as the synthesis of extracellular matrix (ECM) proteins are very sensitive to the surface properties, the characteristics of a biomaterial surface should provide conditions for promoting appropriate cellular functions [2–4].

NiTi, a nickel–titanium alloy, is a quite new material in medical applications with a long history in technical science [5]. It has many unique properties, e.g. shape memory and superelasticity, both based on a thermoelastic, reversible martensitic transformation [6], distinguishing it from any other biomedical material used. In endosseous implants, such as NiTi, the contact area of the implant surface and the bone tissue forms an interacting zone. Similarly to titanium (Ti) and Ti-alloys, NiTi surface is always covered by a natural thin layer of oxide [7]. The function of surface oxides as a protecting film preventing allergic and toxic effects of nickel (Ni) in NiTi has been emphasized in many publications [7–10]. According to these, uniform thick TiO₂-based surface layer minimize the nickel release compared to thinner oxide layer hence improving the biocompatibility of the material. Straightforward, a hypothesis can be made to allege that metal biomaterials should have thick oxide layer to prevent harmful effects to surrounding tissue.

In this report, the main objective was to study if the thickness of the TiO₂-based layer truly has cell protective properties as hypothesized in many publications [11–13]. We used fluorescently labeled cytoskeletal protein paxillin [14, 15] to quantitatively analyze the spatial state of focal adhesions in osteoblastic cells on different oxide thicknesses. In addition, the viability of the cells was studied by quantifying the live and dead cells on the different NiTi surface conditions. As a

V. Muhonen (✉) · J. Tuukkanen
Department of Anatomy and Cell Biology, University of
Oulu, P.O. Box 5000, 90014 Oulu, Finland
e-mail: virpi.muhonen@oulu.fi

V. Muhonen · R. Heikkinen · A. Danilov · T. Jämsä
Department of Medical Technology, University of Oulu,
P.O. Box 5000, 90014 Oulu, Finland

result, we demonstrated that the average number and size of focal adhesions that contained paxillin were strongly affected by the oxidation state of the underlying NiTi alloy. These modified surfaces of NiTi also had a clear effect on cell survival and size. Surprisingly, these cellular responses were contradictory to many of the previously published results. In addition, oxidation process changed to some extent the physical properties of the NiTi alloy.

2 Materials and methods

2.1 Test materials and surface modifications

Fifteen disks of 6 mm-in-diameter and 4 mm-in-height were made of hot-rolled binary NiTi alloy (55.7% Ni and 44.3% Ti by weight). The samples were ground by different silicon emery papers and polished with chromium oxide paste. The test materials were washed with detergent, rinsed, ultrasonically cleaned and finally degreased with 70% ethanol. All the samples were in austenitic state at the temperatures used in biological tests (ranging from +21 to +37°C).

An additional 40 mm-in-diameter NiTi sample (5 mm-in-height) for biological test and flat NiTi samples of $15 \times 15 \times 2 \text{ mm}^3$ in dimensions for X-ray diffraction analysis were also made and handled as the 6 mm-in-diameter samples.

Six of the 6 mm-in-diameter NiTi disks were left untreated, thus having only the natural thin oxide layer at the metal alloy surface. To study the effect of oxide thickness on cell responses, rest of the 6 mm-in-diameter samples were divided into two groups: the first group (5 disks) was oxidized in air during 2 h at 350°C and the second group (4 disks) at 450°C, respectively. Hereafter, the non-treated sample type is called austenite, referring to the phase state of the alloy. The disks treated at 350°C are referred as straw colored (SCO, straw-colored oxide) and the ones oxidized at 450°C as blue colored (BO, blue-colored oxide) corresponding to the color of the disks after the heat treatment. The additional 40 mm-in-diameter sample was oxidized at 600°C during 2 h. Before biological tests the disks were sonicated, degreased with 70% ethanol and autoclaved at 120°C for 20 min. The NiTi samples were ready to use after cooling to room temperature.

To control differences in electrical properties of oxides, special flat samples $80 \times 10 \times 2 \text{ mm}^3$ and samples made of thin (0.5 mm-in-thickness) NiTi wire were used. These groups of samples were oxidized

simultaneously with the samples for biological tests and X-ray diffraction analysis.

2.2 Surface roughness

Surface roughness was measured from atomic force microscopy (AFM) images. AFM imaging was conducted in air with a commercial atomic force microscope (Explorer, Thermomicroscopes, Sunnyvale, CA, USA). Images were collected in contact mode using triangular silicon nitride cantilevers (Veeco Instruments, USA) with a z-scanner of 13.6 μm range. Image resolution was 300×300 . SPMLabNT software version 5.01 (Thermomicroscopes, Sunnyvale, CA, USA) was used to calculate the surface roughness from first-order plane leveled images. The analyzed image size was $100 \times 90 \mu\text{m}$. The numbers of analyzed images were 40 for austenitic sample type, 60 for BO and 80 for SCO. The surface roughness was determined as the average roughness.

2.3 X-ray diffraction analysis

The phase composition of surface layers before and after oxidation was controlled by X-ray diffraction analysis (XDA), using filtered CuK_α radiation. To analyze the structure of the upper surface layer in comparison with that of the basic material, the grazing beam of 1° incidence was used along with the usual one when $2\theta-\theta$ angle relation was complied. The crystal lattice parameters were determined by extrapolation to $\theta = 90^\circ$ using extrapolating function $f(\theta) = 1/2(\cos^2\theta/\theta + \cos^2\theta/\sin\theta)$. The shifts of diffraction lines under grazing beam were controlled by additional experiments when a thin layer of vacuum annealed fine tungsten powder was used as a reference at the surface of oxidized samples. Necessary corrections were applied. The diffraction peaks that did not correspond to austenite, martensite or Ni_3Ti were used as primary information for interpretation of surface oxides phase compositions and structure.

2.4 Electrical resistance measurements

The differences in electrical properties of oxides were assessed by changes in electrical resistance before and after oxidation. The measurements of electrical resistance were performed with industrial digital milliohm meter MEGGER BT51 (Megger, USA) for the flat samples and with specially designed circuit for the wire samples. The specific resistance (resistivity) of the material surface layers after oxidation was determined by gradual etching with simultaneous control of

changes in the samples electrical resistance and thickness considering that the resistances of removed layer and remained material as parallel connected.

2.5 Calculation of oxide thickness

Oxide thickness (δ) after 2 h of oxidation was computed from the sample mass gain per area unit in accordance with the formula

$$\delta = \Delta m / \rho,$$

where Δm is mass augmentation per sample area unit and ρ is oxide density. This approach was based on the assumption that the mass gain was a result of oxygen adsorption only, and that all of this oxygen was used to produce the TiO_2 oxide. The validity of this assumption was confirmed by the results of X-ray diffraction (XRD) surface phase control, which demonstrated the predominant content of TiO_2 (rutile) in the surface phase composition after all oxidation temperatures used. The value of $\rho = 4.2 \text{ g/cm}^3$ for stoichiometric TiO_2 (rutile) [16] was used. To provide higher accuracy of determination for the small mass augmentations after 2 h of oxidation, their values were interpolated from the equations fitted to the experimental data mass gain versus oxidation time.

2.6 Cell culture

Rat osteosarcoma cell line ROS-17/2.8 (a generous gift from G. A. Rodan, Merck Research Laboratories, West Point, PA, USA) was used for the experiments. The cells were cultured at 37°C in a humidified atmosphere (5% CO_2 , 95% air) in alpha minimal essential medium (α MEM, Gibco), supplemented with 10% fetal calf serum (Bioclear), antibiotics (100 U of penicillin/mL, 100 μg of streptomycin/mL) and L-glutamine (2 mM). The cultures were allowed to reach confluence before subculturing onto the NiTi discs.

The cells were washed with phosphate-buffered saline (PBS) and trypsin–EDTA was added to detach adherent cells. The 6 mm-in-diameter discs were placed individually on 24-well plate and 5×10^3 cells were seeded per disc and allowed to attach for 3 h at 37°C before 1 mL complete medium per well was added. The cells were allowed to grow for 48 h before fixation with 3% (w/v) paraformaldehyde (PFA) or staining with a cytotoxicity test kit. The separate large NiTi disk (oxidized at 600°C) was treated the same way, but due to the larger surface area, 3×10^4 cells were seeded onto the disk and 10 mL complete medium was added after the 3 h attachment.

2.7 Immunofluorescence staining and visualization of focal adhesions

The PFA-fixed cells were permeabilized with 0.1% (v/v) Triton-X-100 in PBS for 10 min on ice followed by treatment with 0.2% BSA for 30 min at room temperature. The cells were stained by using mouse monoclonal paxillin antibody (ZYMED Laboratories, San Francisco, CA, USA) at 1:100 in PBS for 45 min on ice. Staining was carried out with secondary antibodies (ALEXA Fluor 488 goat anti-mouse IgG, Molecular Probes, Oregon, USA) for 30 min on ice. To visualize the nuclei, the cells were incubated with DNA-binding fluorochrome Hoechst 33258 (1:1,000) for 10 min at room temperature.

The focal adhesions were studied under a confocal microscope LSM 510 equipped with an inverted microscope Axiovert 100M and 63 \times objective (NA 1.2/water, Zeiss, Germany). From each 6 mm-in-diameter disc, 8 frames were randomly scanned with $1,024 \times 1,024$ frame size (pixel size $0.14 \times 0.14 \mu\text{m}$). Nineteen frames were scanned from the additional large NiTi disk oxidized at 600°C . These optical sections were scanned next to the metal alloy surface at the level containing approximately most of the focal adhesions.

2.8 Quantification of focal adhesions

The numbers of focal adhesions were measured with a digital image analyser (MCID M4 3.0 Rev. 1.1, Imaging Research Inc., Canada). The measured area of interest was $146.2 \times 146.2 \mu\text{m}$, corresponding to one confocal microscope field. The confocal microscope images were segmented on green color intensity, hue and saturation, representing the emission color of the secondary antibody. These interactively defined paxillin-containing focal adhesions were automatically counted from the region of interest. All defined areas of one pixel in size were excluded from the automatic count. The total number of analyzed confocal pictures (after three experimental runs) was 134 for austenite, 111 for SCO and 93 for BO sample type. From the large NiTi disk 19 fields were analyzed. The average number of cells per field was also calculated, and with the knowledge of the average number and areas occupied by the focal contacts per confocal image, the number and coverage of focal plaques per cell was estimated.

2.9 Cytotoxicity test

The ROS-17/2.8 cells cultured 48 h on the NiTi samples were washed with PBS and stained with a LIVE/DEAD[®] Viability/Cytotoxicity kit (Molecular

Probes, Oregon, USA). This assay is based on the simultaneous determination of live and dead cells with the detection of intracellular esterase activity by calceinAM and plasma membrane integrity for ethidium homodimer-1 (EthD-1), respectively. The optimal concentrations of the EthD-1 dye were 0.1 μM and for the calceinAM dye 1.0 μM [17].

Stained cells were immediately viewed under confocal microscope LSM 510 (10 \times objective NA 0.45/water). For each disk, five pictures were taken from randomly chosen areas (1,024 \times 1,024 frame size, pixel size 0.9 \times 0.9 μm). These optical sections were scanned from the most descriptive focal plane, illustrating the stained cells in that area of interest as well as possible. The confocal microscope images were analyzed with digital image analyser. The measured area of interest was 921.3 \times 921.3 μm . From each image, the numbers of live and dead cells were calculated and differences between sample groups were estimated. The proportional area (per one confocal field) occupied by live cells was also obtained—that is the spreading of live cells on the test surfaces. The total number of analyzed pictures (after three experimental runs) was 91 for austenite, 75 for SCO and 60 for BO sample type. Cytotoxicity test was not performed to the large NiTi sample oxidized at 600°C.

2.10 Statistical analysis

Mean values and standard deviations (SD) were computed. Analysis of variance (ANOVA) and Student's *t*-test were utilized to assess the level of significance of the differences between the experimental groups. Probabilities of $p < 0.05$ were considered significant. All statistical analyses were performed with commercial software (Origin 5.0 and 6.0, Microcal Software, Inc., USA).

3 Results

3.1 Surface roughness

The mean roughness of the artificially oxidized samples was 0.262 μm for SCO and 0.310 μm for BO. The average surface roughness for non-oxidized austenitic

NiTi was 0.849 μm . Statistical analyses showed that the austenite samples were significantly rougher than the oxidized surfaces ($p < 0.001$). Smaller difference was found between the BO and SCO disks ($p < 0.01$).

3.2 X-ray diffraction

The X-ray patterns obtained under (θ – θ conditions showed that the non-oxidized NiTi was characterized in the initial state by B2 crystal structure (austenite) with small quantities of Ti_2Ni . The basic phase in the bulk of NiTi after its oxidation at 350°C and at 450°C was also austenite, but quantities of martensitic B19' phase in comparison to the initial state was present in alloy structure. The intensities ratios for the strong austenitic and martensitic lines demonstrated that the alloy structure after oxidation at 450°C contained higher amounts of martensite in comparison to that after oxidation at 350°C. Data obtained from X-ray experiments with grazing beam demonstrated that the metal alloy next to the oxide layer had different phase composition than the bulk. After oxidation at both temperatures these layers contained higher amounts of martensite than the bulk of the alloy.

3.3 Electrical resistance

The experiments showed that the electrical resistance changes as a result of sample oxidation (Table 1). To characterize the electrical properties of oxides the average resistivity was calculated from the differences in oxidized sample resistance before and after etching, thus considering the electrical resistances of the oxide layer and the bulk material as parallel connected. Table 1 represent the electrical properties of the basic material and oxidized surface after 1 h oxidation. Note the different signs in the results of the change in resistivity when comparing NiTi in initial stage and after oxidation.

3.4 Oxide thickness

The plots of mass gain per surface area unit (Δm) as a function of time for NiTi samples oxidized at 350, 450

Table 1 Changes in electrical resistance (ΔR) of NiTi samples as a result of their oxidation, and resistivity of basic NiTi alloy (ρ_{NiTi}) and oxide layers (ρ_{ox})

Oxidation temperature (°C)	ΔR (ohm)	ρ_{NiTi} (initial) ($\times 10^{-6}$ ohm m)	ρ_{NiTi} (after oxidation) ($\times 10^{-6}$ ohm m)	Change in ρ_{NiTi} ($\times 10^{-6}$ ohm m)	ρ_{ox} ($\times 10^{-6}$ ohm m)
350	0.107	0.769	0.804	–0.035	2.61
450	0.019	0.791	0.770	0.021	8.48

and 600°C demonstrated that NiTi oxidation followed logarithmic time dependence at 350°C and parabolic dependence at 450 and 600°C. The experimental oxidation curves were described by the following equations:

$$\Delta m = 0.2205 \times 10^{-4} \times lgt \text{ for oxidation at } 350^\circ\text{C}, \quad (1)$$

$$\Delta m^{1.67} = 0.83311 \times 10^{-8} \times t \text{ for oxidation at } 450^\circ\text{C}, \quad (2)$$

$$\Delta m^2 = 4.744 \times 10^{-8} \times t \text{ for oxidation at } 600^\circ\text{C}. \quad (3)$$

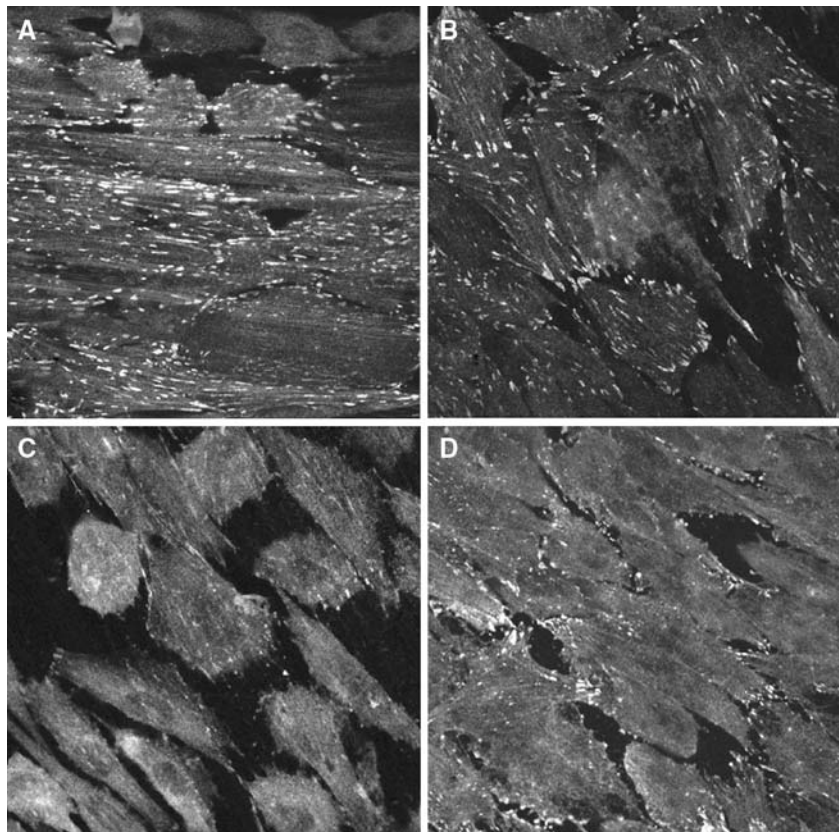
The related augmentations of oxide thickness (δ) after 2 h of oxidation were calculated from the Eqs. 1–3. Oxide thicknesses were: 15.6 nm for SCO, 51.0 nm for BO and 725.0 nm for the additional NiTi sample oxidized at 600°C. Despite limitations conditioned by the use of constant oxide density, the values of oxide thicknesses estimated in the present study were consistent with the oxide thickness obtained by direct measurements in a study for similar oxidation regimes [12]. Since the oxides after oxidation included

the initial natural oxide layer of non-oxidized NiTi, the final values should be summarized with the initial oxide thickness (δ_0). This is also the oxide thickness for the austenite samples. In the absence of available methods for its determination in the present study, we ascribed to δ_0 the value of 5 nm, which was the spontaneous oxide crystal size. Approximately the same value (about 3 nm) was described by the theory [18] and has been reported for mechanically polished NiTi [19].

3.5 Cell attachment

Figure 1 represents images of ROS-17/2.8 osteoblastic cells at the surface of the different NiTi alloy samples. It is evident, that focal adhesion formation and their average size is reduced when cells are grown on NiTi surface oxidized at 450°C and 600°C (Fig. 1C and D) compared to the other sample types. Despite the fact that these BO NiTi disks and the one oxidized at 600°C contained the thickest surface oxide layers (56.0 nm for BO and 730.0 nm for 600°C oxidation), the cells seemed to attach best to the surface with a quite thin oxide layer (20.6 nm, Fig. 1B) or to the surface that lacks artificially produced oxide layer (Fig. 1A).

Fig. 1 Immunofluorescence staining of focal adhesion with paxillin antibody on ROS-17/2.8 cells. **(A)** Austenitic NiTi, **(B)** NiTi oxidized at 350°C (SCO), **(C)** at 450°C (BO) and **(D)** at 600°C. Numerous white patches represent focal adhesion plaques. The average thickness of the surface oxide layer: **(A)** 5.0 nm, **(B)** 20.6 nm, **(C)** 56.0 nm and **(D)** 730.0 nm. Magnification 63×, frame size 146.2 × 146.2 μm



The results of cell adhesion studies in the austenite, SCO and BO surface conditions are summarized in Fig. 2. The average number of focal adhesions per cell was significantly ($p < 0.001$) higher in the austenitic and SCO samples compared to the BO ones (Fig. 2A). Statistical analyses showed also a difference between SCO and austenite samples ($p < 0.01$). Based on these results, it seems that SCO surface had the highest number of focal adhesion per cell. The average area (μm^2) occupied by focal adhesions, i.e. the size of focal adhesions in a cell, or in an other way, the area of cell

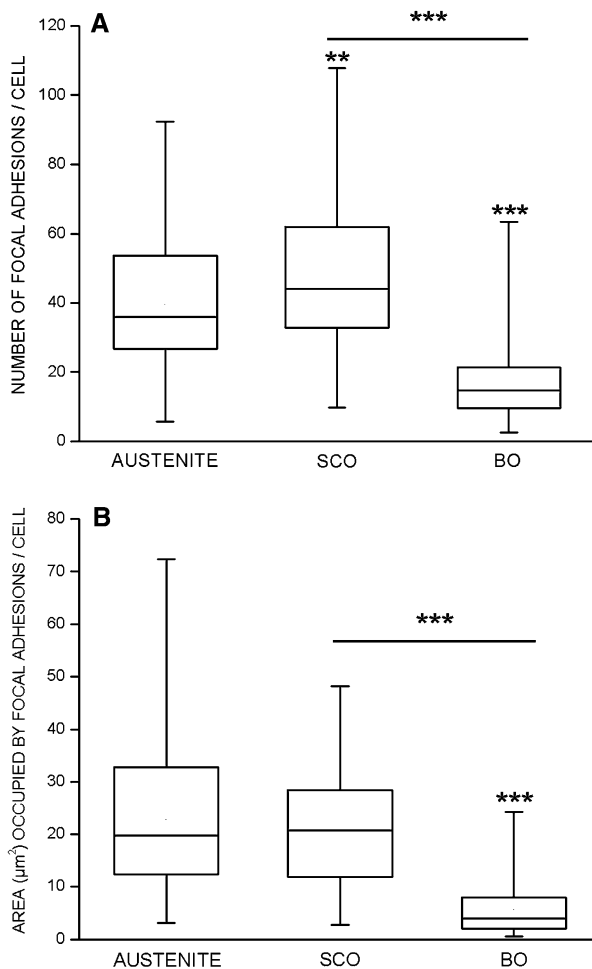


Fig. 2 (A) The average number of focal adhesions per ROS-17/2.8 cell. The mean values of focal adhesions differ very significantly ($p < 0.001$) between austenitic and BO (oxidized at 450°C), and also between SCO (oxidized at 350°C) and BO NiTi groups. Difference in the amount of focal adhesion plaques was also observed between austenite and SCO disks ($p < 0.01$). (B) The total area (μm^2) of focal adhesions per ROS-17/2.8 cell. Statistical differences between austenite and BO and between SCO and BO were observed ($p < 0.001$). The results are combined from three experimental runs. The analyzed numbers of confocal images were: austenite = 134, SCO = 111 and BO = 93. Each field had approximately 20 cells. *** $p < 0.001$; ** $p < 0.05$

membrane attach to NiTi surface, was similarly higher in austenitic and SCO samples compared to the NiTi treated in 450°C ($p < 0.001$, Fig. 2B).

It is highly important to remark that the average number of cells per a confocal image after the 48-h culturing period was statistically identical between the different sample types. So the differences observed did not depend on differences in the cell amount, but truly were differences between focal adhesion number and size between sample types. The total average number of cells after 48 h was 1,100 on the austenite, SCO and BO NiTi disks. This also means that a major part of the cells originally seeded onto the samples (5×10^3 cells per disc) did not attach. These cells were probably flushed away from the NiTi button when culturing media was added.

The additional 40 mm-in-diameter sample was also analyzed. The results showed the same decreasing trend as seen in the other NiTi samples. The number of focal adhesions was approximately 16 plaques per cell and the area covered by them was approximately $11 \mu\text{m}$.

3.6 Cytotoxicity test

The results of the cytotoxicity assay demonstrated that most of the cells grown on oxidized NiTi surfaces were alive (Fig. 3A) and only a small portion of the cells were dead (Fig. 3C). This was predictable, since NiTi is considered to be non-cytotoxic [17]. There was a significant difference ($p < 0.001$) in the number of live cells between the austenite and SCO sample groups (Fig. 3A), indicating that SCO surface had the largest percentage of live cells of the three surfaces studied. In addition, the cells were significantly smaller in NiTi disks oxidized at 450°C ($p < 0.05$) compared to other surface conditions (Fig. 3B, results presented per confocal image). The SCO NiTi had the smallest fraction of dead cells (Fig. 3C). The difference was statistically highly significant ($p < 0.001$) when compared to the austenitic sample type. Nonetheless, the observed differences in the percentage of dead cells between the three different sample types and the overall number of dead cells were still quite small.

4 Discussion

In this study, we investigated the effect of different levels of NiTi surface oxidation on osteoblastic cell attachment and survival in order to reveal the influence of the thickness of the oxide layer on these cellular functions. It was clear from our results that straight

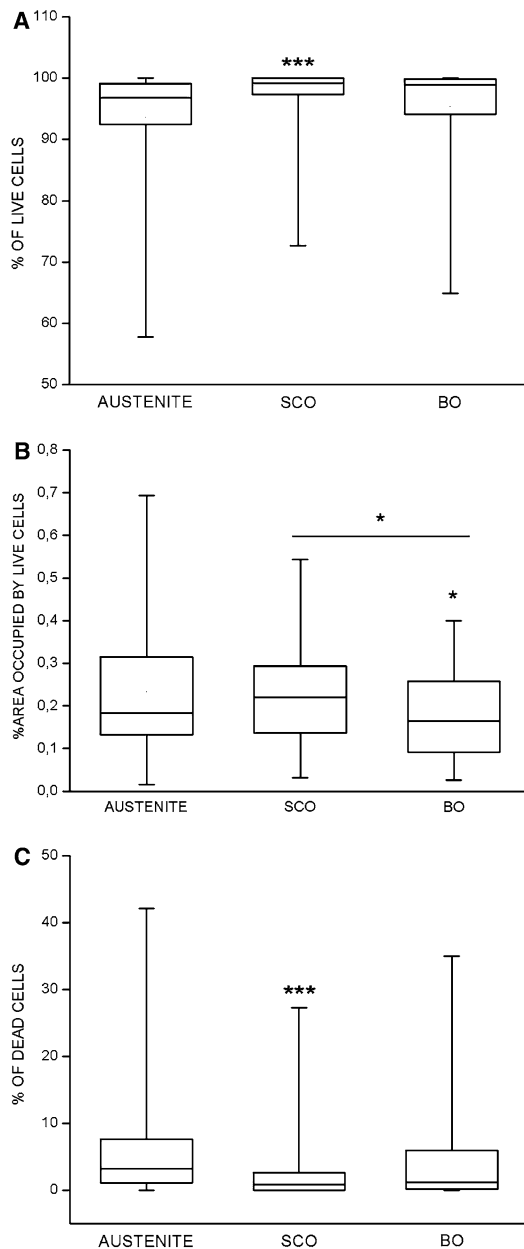


Fig. 3 Results of the cytotoxicity test. **(A)** The percentages of live cells in the ROS-17/2.8 cell populations on the three different NiTi alloy samples. Statistical analyses showed a significant difference in the percentages between SCO and austenite NiTi disks ($p < 0.001$). **(B)** The proportional area occupied by live cells. The mean values differ significantly between austenitic and BO (oxidized at 450°C) sample groups ($p < 0.05$). A similar difference is also observed between the oxidized samples. These results are presented per one microscopy field ($921.3 \times 921.3 \mu\text{m}$). **(C)** The percentages of dead cells in the ROS-17/2.8 cell populations on the three sample groups. A significant difference in the amount of dead cells between austenitic and SCO NiTi was observed ($p < 0.001$). The results are combined from three experimental runs. The analyzed numbers of confocal images were: austenite = 91, SCO = 75 and BO = 60. *** $p < 0.001$; * $p < 0.05$

correlation between oxide layer thickness and cellular well-being cannot be made.

Cell adhesion to extracellular substratum is, to a great extent, mediated by integrins; a heterodimeric family of cell surface receptors [20]. Integrins are directly associated via their cytoplasmic domains of β -integrin subunits with the actin cytoskeleton through a complex submembrane assembly of structural proteins, such as talin and paxillin [21]. These proteins, in addition with different signalling proteins, constitute the diverse variety of focal adhesion complexes. Our results showed that the amount and size of paxillin containing focal adhesions deteriorates in ROS-17/2.8 osteosarcoma cells in correlation with surface oxide thickness. This deterioration of cell attachment to the underlining NiTi surface was not the outcome of different cell numbers between sample types, since the average number of cells was the same between austenite, SCO and BO NiTi samples.

In addition, as support evidence, one NiTi sample was oxidized at 600°C and tested during the procedures previously described. This sample type should not only have the thickest oxide layer in the range of temperatures used for oxidation [18], but its surface is enriched by Ti as well [19]. The sample was included to the experiments in intention to see if this kind of surface promotes cell attachment as indirectly presumed in [22] and directly predicted in [19]. Analogous to our other results, the extra NiTi sample showed inadequate focal adhesion formation.

The results of the cytotoxicity test showed that in all the tested surfaces the percentages of live cells were high. The cell size appeared to be significantly larger on the non-oxidized surface and on the samples oxidized at 350°C when compared to the samples with the thickest oxide surface. It can be hypothesized, that the small cell size on the BO NiTi demonstrate slow growth rate. Although the cell spreading on this sample type was not completely suppressed, the confluence of the cells was distinctively smaller compared to the other surface conditions. The number of observed dead cells was smaller in samples oxidized at 350°C compared to the austenitic sample. The interpretation of this result needs caution, since detached dead cells are easily removed from the surface and thus the observation of dead cells might be somewhat misleading.

We cannot rule out the possible effects of roughness on these adhesion results, since statistical analyses clearly showed differences in this surface parameter between the three NiTi surface conditions. But the effect of these differences on cellular behavior is

probably small, since subtle difference in focal adhesion length and no differences in focal adhesion movement was observed with titanium samples having much larger roughness differences (ranging up to 6.07 μm) [23]. In this study, the roughness varied at the most only approximately 0.6 μm .

A recent study [24] has shown that cell attachment is in strong dependence on the surface ability to adsorb extracellular matrix (ECM) proteins. High ability to adsorb proteins, in particular vitronectin (Vn) and fibronectin (Fn), leads to better cell attachment on biomaterials. On the other hand, poor adsorption of proteins leads to cAMP dependent cell aggregation and suppression of cell spreading and growth rate [25]. The physical state of the ECM alters the properties of cell–matrix adhesions [26]. Different biomaterial surface properties are reflected to the ECM, in particular to the molecular architecture of the ECM, including protein conformation [27–29]. This directly influences the cells ability to form adhesions complexes, and ultimately affects many aspects of cell behavior. In this connection, the results obtained in the present study allow to suggest that the observed differences in cell behavior were conditioned by different abilities of oxidized surface to adsorb proteins. An example of heat-treatment effect on protein adsorption onto TiO_2 was earlier reported in [30]. Volkenstein [31] studied the factors affecting the adsorption ability of semiconductor film on a metal surface. He showed that any chemical or structural change taking place in the oxide surface and/or in the bulk metal (that is in contact with the oxide) will give rise to changes in the adsorption ability.

The changes in the amount of martensite next to the oxide layer of NiTi could be the main reason for changes in the conditions at the oxide–metal contact, since Gibbs energies of austenite and martensite are different [32]. Thus the changes in oxide–metal contact potential caused by alterations in phase composition could lead to variations in external surface potential. The changes in surface Fermi level should affect the surface adsorption ability. The different outcome of electrical resistance after oxidation in the two temperatures along with the results of cell attachment demonstrated the correlation between surface electrical properties and cell attachment. Furthermore, the results of the additional sample oxidized at 600°C revealed not only different value of the electrical resistance, but different sign as well ($\Delta R = -0.087 \text{ ohm}$).

Our analyses showed that that crystal lattice strain was remarkably different between the oxidized samples (350, 450 and 600°C). This means that the lattice distortions between the oxidized samples are different. Hence, the stresses exerted on the surface of the NiTi

samples are different between the sample types investigated. This might have more pronounce effect on cellular behavior, instead of the TiO_2 -based surface oxide layer, which might only have a secondary contribution on the biocompatibility of NiTi alloy. Although NiTi surface oxide layer might have some protective effects on cells, our results indicate that the possibility of directly enhancing biocompatibility of a medical (metal) material merely with thickening the surface oxide layer is not probably worth excessive research, but detailed studies are needed for clarifying the real factors behind successful implant–tissue interaction.

Acknowledgments The authors thank Ms. Taina Poikela for technical assistance. This work was supported in part by the National Technology Agency of Finland (40245/03). V. M. was supported by the National Graduate School for Musculoskeletal Diseases in Finland.

References

1. L. G. GRIFFITH, *Ann. N Y Acad. Sci.* **961** (2002) 83
2. Z. SCHWARTZ and B. D. BOYAN, *J. Cell. Biochem.* **56** (1994) 340
3. J. Y. MARTIN, Z. SCHWARTZ, T. W. HUMMERT, D. M. SCHRAUB, J. SIMPSON, J. LANKFORD Jr, D. D. DEAN, D. L. COCHRAN and B. D. BOYAN, *J. Biomed. Mater. Res.* **29** (1995) 389
4. R. K. SINHA, F. MORRIS, S. A. SHAH and R. S. TUAN, *Clin. Orthop.* **305** (1994) 258
5. W. J. BUEHLER and F. E. WANG, *Ocean Eng.* **1** (1968) 105
6. T. SABURI, in “Shape memory materials”, edited by K. OTSUKA and C. M. WAYMANN (Cambridge University Press, New York, 1998), p. 49
7. D. M. BRUNETTE, P. TENGVALL, M. TEXTOR and P. THOMSEN, “Titanium in medicine” (Springer-Verlag, Berlin-Heidelberg-New York, 2001), p. 171
8. J. VAN HUMBEECK, R. STALMANS and P. A. BESSELINK, in “Metals as biomaterials”, edited by J. A. HELSEN and H. J. BREME (Chichester-Wiley, 1998), p. 73
9. D. J. WEVER, A. G. VELDHUIZEN, J. DE VRIES, H. J. BUSSCHER, D. R. UGES and J. R. VAN HORN, *Biomaterials* **19** (1998) 761
10. S. D. PLANT, D. M. GRANT and L. LEACH, *Biomaterials* **26** (2005) 5359
11. S. TRIGWELL, R. D. HAYDEN, K. F. NELSON and G. SELVADURAY, *Surf. Interface Anal.* **26** (1998) 483
12. G. S. FIRSTOV, R. G. VITCHEV, H. KUMAR, B. BLANPAIN and J. VAN HUMBEECK, *Biomaterials* **23** (2002) 4863
13. D. A. ARMITAGE, T. L. PARKER and D. M. GRANT, *J. Biomed. Mater. Res.* **66A** (2003) 129
14. M. C. BECKERLE, *J. Cell Biol.* **103** (1986) 1679
15. C. E. TURNER, J. R. GLENNEY Jr and K. BURRIDGE, *J. Cell Biol.* **111** (1990) 1059
16. ASTM Diffraction Data File (ASTH, Philadelphia, 1969), 73-2224, 21-1276
17. A. KAPANEN, J. ILVESARO, A. DANILOV, J. RYHÄNEN, P. LEHENKARI and J. TUUKKANEN, *Biomaterials* **23** (2002) 645

18. P. Kostad, “High-temperature oxidation in metals” (Wiley, New York), p. 966
19. D. A. ARMITAGE and D. M. GRANT, *Mater. Sci. Eng. A00* (2003) 89
20. R. O. HYNES, *Cell* **48** (1987) 549
21. E. ZAMIR and B. GEIGER, *J. Cell Sci.* **114** (2001) 3583
22. O. CISSE, O. SAVADOGO, M. WU and L. H. YAHIA, *J. Biomed. Mater. Res.* **61** (2002) 339
23. A. DIENER, B. NEBE, F. LUTHEN, P. BECKER, U. BECK, H. G. NEUMANN and J. RYCHLY, *Biomaterials* **26** (2005) 383
24. N. FAUCHEUX, R. SCHWEISS, K. LUTZOW, C. WERNER and T. GROTH, *Biomaterials* **25** (2004) 2721
25. N. FAUCHEUX and M. D. NAGEL, *Biomaterials* **23** (2002) 2295
26. B.-Z. KATZ, E. ZAMIR, A. BERSHADSKY, Z. KAM, K. M. YAMADA and B. GEIGER, *Mol. Biol. Cell* **11** (2000) 1047
27. A. J. GARCIA, M. D. VEGA and D. BOETTIGER, *Mol. Biol. Cell* **10** (1999) 785
28. R. THULL, *Biomol. Eng.* **19** (2002) 43
29. B. G. KESELOWSKY, D. M. COLLARD and A. J. GARCIA, *J. Biomed. Mater. Res.* **66** (2003) 247
30. H. NYGREN, P. TENGVALL and I. LUNDSTRÖM, *J. Biomed. Mater. Res.* **34** (1997) 487
31. F. F. VOLKENSTEIN (Nauka, Moscow, 1973), p. 234 (in Russian)
32. C. M. WAYMAN, in “Proceedings of the international symposium on shape memory effects and applications, Toronto, 1975”, edited by J. Perkins (Plenum Press, New York, 1975)